УДК 551.465

© *Г. Вяли*[1], *В. М. Журбас*[2], *Я. Лаанеметс*[1], *У. Липс*[1]
[1]Таллинский технический университет, г. Таллин, Эстония
[2]Институт океанологии им. П. П. Ширшова РАН, г. Москва
germo.vali@msi.ttu.ee

КЛАСТЕРИЗАЦИЯ ПЛАВАЮЩИХ ЧАСТИЦ ИЗ-ЗА СУБМЕЗОМАСШТАБНОЙ ДИНАМИКИ: МОДЕЛЬНОЕ ИССЛЕДОВАНИЕ ДЛЯ ФИНСКОГО ЗАЛИВА БАЛТИЙСКОГО МОРЯ

Статья поступила в редакцию 04.12.2017, после доработки 18.04.2018.

Поле скорости, симулируемое моделью циркуляции с чрезвычайно высоким горизонтальным разрешением (шаг сетки 232×232 м) в Финском заливе в течение летних событий апвеллинга, используется для расчета адвекции плавающих лагранжевых частиц, равномерно распределенных на поверхности моря первоначально. Обнаружено, что в течение относительно короткого времени адвекции τ (порядка одного дня) частицы собираются в узких удлиненных полосах, характеризующихся чрезвычайно высокими положительными значениями завихренности, конечно-временного показателя Ляпунова и горизонтальных термохалинных градиентов (фронты). Скорость кластеризации, определяемая как временная производная стандартного отклонения нормализованной концентрации частиц, при малом значении τ асимптотически стремится к стандартному отклонению дивергенции скорости течения на поверхности. Стандартное отклонение дивергенции скорости, в свою очередь, демонстрирует значительный рост с уменьшением шага сетки, подтверждая первостепенную роль субмезомасштабной динамики в кластеризации плавающего материала. Показано, что при большом значении τ функция плотности вероятности концентрации плавающих частиц стремится к логнормальности. На основе интегрирования конвергенции скорости по траектории материальной частицы назад по времени, сформулирован критерий кластеризации за конечный промежуток времени.

Ключевые слова: плавающие частицы, лагранжевы когерентные структуры, конечно-временной показатель Ляпунова, кластеризация, прибрежный апвеллинг, Балтийское море, субмезомасштаб.

G. Väli[1], *V. M. Zhurbas*[2], *J. Laanemets*[1], *U. Lips*[1]
[1]Tallinn University of Technology, Department of Marine Systems, Tallinn, Estonia
[2]Shirshov Institute of Oceanology, Moscow, Russia

CLUSTERING OF FLOATING PARTICLES DUE TO SUBMESOSCALE DYNAMICS: A SIMULATION STUDY FOR THE GULF OF FINLAND, BALTIC SEA

Received 04.12.2017, in final form 18.04.2018.

Velocity field simulated by a circulation model with extremely high horizontal resolution (the grid bin is 232×232 m) in the Gulf of Finland during a period of summer upwelling events is used to calculate advection of floating Lagrangian particles that are uniformly distributed on the sea surface initially. For a relatively short time of advection τ (of the order of one day), the particles are found to gather within narrow, elongated stripes characterized by extremely high, positive values of vorticity, Finite-Time Lyapunov Exponent, and lateral thermohaline gradients module (fronts). The clustering rate, defined as the time derivative of the standard deviation of normalized particle concentration, tends asymptotically at small τ to the standard deviation of flow divergence. The standard deviation of flow divergence, in its turn, displays a considerable growth with the refinement of the model grid, confirming the paramount role of submesoscale dynamics in clustering of floating stuff. At large τ, the probability density function of floating particle concentration is shown to tend to lognormality. Based on the backward-time integration of the Lagrangian velocity convergence, a criterion for finite-time clustering is introduced.

Key words: floating particles, Lagrangian Coherent Structures, Finite-Time Lyapunov Exponent, clustering, coastal upwelling, Baltic Sea, submesoscale.

Ссылка для цитирования: *Вяли Г., Журбас В. М., Лаанеметс Я., Липс У.* Кластеризация плавающих частиц из-за субмезомасштабной динамики: модельное исследование для Финского залива Балтийского моря // Фундаментальная и прикладная гидрофизика. 2018. Т. 11, № 2. С. 21—35.

For citation: *Väli G., Zhurbas V. M., Laanemets J., Lips U.* Clustering of floating particles due to submesoscale dynamics: a simulation study for the Gulf of Finland, Baltic Sea. *Fundamentalnaya i Prikladnaya Gidrofizika.* 2018, 11, 2, 21—35.

doi: 10.7868/S2073667318020028

1 Introduction. Under a term of clustering, we imply the ability of floating Lagrangian particles (surface drifters), that are uniformly distributed on the sea surface in the beginning, to gather into some clusters (conglomerates, coherent structures), in the course of their advection by currents. This process is thought to contribute to the formation of complex structures of phytoplankton distribution observed on remote sensing images, especially at meso- and submesoscales e.g. [1—3, 4] determined spiral cyclonic eddies with a mean diameter about 7 km on satellite radar images mainly during spring and summer phytoplankton blooms in the Baltic Sea. Also, it is of practical importance in relation to forecast of pollutant fields on the sea surface, e.g. [5].

The Gulf of Finland, an elongated and relatively shallow basin (about 400 km long, 48—135 km wide, mean depth 37 m) lies in the north-eastern part of the Baltic Sea (fig. 1). The freshwater discharge, mainly the Neva River (an average runoff 77.6 km^3 yr^{-1} [6]) in the eastern part and spreading of saltier north-eastern Baltic Proper water (8—11 g kg^{-1}) into the deep layer maintain the strong haline stratification with the halocline at the depths of 60—70 m. Surface salinity decreases from 6—7 g kg^{-1} at the entrance to about 1 g kg^{-1} in the Neva estuary. The thermal stratification has a seasonal character and summer thermocline settles at a depth of 10—15 m starting from May (e.g. [7]). The Gulf of Finland is an area of the Baltic Sea known for frequent summer coastal upwelling events. Upwelling characteristics, dynamics and related nutrient transport were investigated in the Gulf of Finland using satellite sea surface temperature imagery, in situ measurements and model simulations (e.g. [8—15]).

The submesoscale structures are usually related to energetic mesoscale flow field, e.g. [1] and [16—17]. Väli et al. [18] examined submesoscale structures in the Gulf of Finland using high-resolution (grid size 0.125 nautical miles) simulations for series of coastal upwelling events in summer 2006. They found in the surface layer the high Rossby number (Ro>1) cyclonic structures: threads with a width of 2—3 and length of 10—50 km, vortices with a core diameter of 4—6 km, and spiral eddies of 10—15 km diameter. The high potential vorticity threads formed during the development phase, while the cyclonic vortices and spiral eddies during the relaxation phase of upwelling events.

The objectives of this work are (a) to simulate clustering process in the Gulf of Finland based on circulation model of very high (submesoscale) resolution, (b) to find out what factors determine clustering rates; (c) to study evolution of statistical properties of floating particles concentration in the course of clustering, and (d) to compare sea surface images "painted" by the re-distributed floating particles with patterns of submesoscale coherent structures in different Eulerian and Lagrangian fields such as temperature, salinity, density, vorticity, divergence and strain of currents, lateral density gradient module, and Finite Time Lyapunov Exponent.

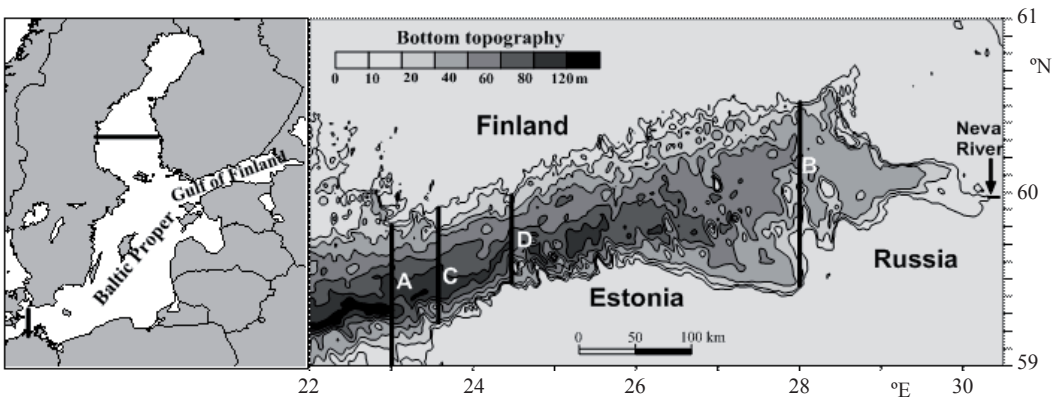

Fig. 1. A map of the Baltic Sea (left panel) and Gulf of Finland (right panel).
Bold black lines (left panel) mark the model domain boundaries at the west and north. Bold black lines (right panel) mark the western (A) and eastern (B) borders of the sea area from where the simulated data are used for the analysis. Black bold lines C and D mark the sea area for the detailed analysis. The bottom topography is drawn from the gridded topography by [24] in meters.

Рис. 1. Карта Балтийского моря (слева) и Финского залива (справа).
Жирные черные линии (слева) обозначают границы области моделирования на западе и севере.
Жирные черные линии (справа) обозначают западную (A) и восточную (B) границы области моря, из которой данные моделирования используются для анализа. Черные жирные линии C и D обозначают морскую зону для детального анализа. Рельеф дна взят из топографии на регулярной сетке [24].

It is worth noting that the ability of clustering of passive tracers on the sea surface of the Gulf of Finland was studied by [19]. The authors introduced a modified measure of finite-time compressibility that accounts for time correlations of realistic flows and is directly related to the ability of clustering of passive tracers in some regions of the sea surface. This measure was evaluated based on 3D velocity fields calculated using a circulation model with 2 nautical mile grid and a code for tracking Lagrangian trajectories. The level of finite-time compressibility reached the threshold of likely formation of patches usually in coastal regions but also in certain elongated offshore areas of the Gulf of Finland. To our minds, results by [19] have to be revisited because they used a circulation model with a too scarce grid that poorly resolved mesoscale motions and did not resolve submesoscale motions at all. Meanwhile, it will be shown below in this paper that mesoscale and especially submesoscale motions can strongly increase the clustering rates.

2 Material and methods

2.1 Model setup. The analysis is based on a high-resolution numerical simulation of upwelling events in the Gulf of Finland for the period of summer 2006 (0.125 nautical miles grid, see [18] for details). Short description of the model and setup is given below. To create sea surface images, simulated values of velocity components, temperature and salinity (u, v, T, S, respectively) from the sea surface were used.

Hydrodynamical model. We applied the ATOP version of the Princeton Ocean Model (POM) (see [20] and [21] for details) in the Baltic Sea. The POM is a primitive equation, sigma coordinate, free surface, hydrostatic model with a second moment turbulent closure sub-model embedded [22]. The model domain included almost whole Baltic Sea to the east of 13°E and south of 62°N and was closed at its western and northern boundaries. The horizontal step of the model grid was 0.125 nautical miles in the Gulf of Finland to the east of 23°E (fig. 1) and 0.5 nautical miles in the rest of the Baltic Sea; there were 60 sigma layers in the vertical. Sub-grid lateral eddy diffusivity was resolved using the Smagorinsky formulation [23]. The digital topography of the Baltic Sea (resolution of 1 nautical mile) is taken from [24] and for the Gulf of Finland (resolution of 0.25 nautical miles) from [25] and [26].

Atmospheric forcing (wind stress and surface heat flux components) was calculated from wind, solar radiation, air temperature, total cloudiness and relative humidity data taken from HIRLAM (High Resolution Limited Area Model) version of the Estonian Weather Service with the spatial resolution of 11 km and forecast interval of 1 h ahead of 54 h, recalculated after every 6 h [27]. Freshwater supply was applied as the average Neva River inflow of 2460 $m^3\ s^{-1}$ [6].

Initial thermohaline fields were taken from HIROMB (High-Resolution Operational Model of the Baltic Sea), a z-level model, from the 1 nautical miles grid step version as provided by SMHI [28].

Model simulations were performed from 10 July to 27 September 2006 covering several upwelling events along both the northern and the southern coast of the Gulf of Finland.

Keeping in mind a very small horizontal step of the model grid in the Gulf of Finland to the east of 23°E, $\delta x = 0.125$ nautical miles, one needs to make sure that the hydrostatic approximation used in POM is still valid. [29] formulated a non-dimensional criterion for hydrostatic motions as

$$\mathbf{n} = \frac{\gamma^2}{\mathrm{Ri}} \langle\langle 1 ,$$

where $\mathbf{n}$ is a so-called non-hydrostatic parameter, $\gamma = H/L$ is the aspect ratio, $\mathrm{Ri} = N^2 H^2/U^2$ is the Richardson number, H and L are characteristic vertical and horizontal scales of a phenomenon with vertical and horizontal velocity scales W and U, respectively. In our case $\delta x = 232$ m for a nested model domain in the Gulf of Finland east of 23°E where the sea depth $H_{\mathrm{sea}} \le 80$ m for more than 95 % of the sea area (see fig. 1). Taking into account that $\mathrm{Ri} > 1$ for large-scale, mesoscale, and even submesoscale motions [1], $H \le H_{\mathrm{sea}}$, and $L > \delta x$, we get

$$\mathbf{n} \langle \gamma^2 \langle \frac{H_{\mathrm{sea}}^2}{(\delta x)^2} = \frac{80^2}{232^2} = 0.12 \langle\langle 1 .$$

Therefore, the hydrostatic approximation is satisfied with reasonably high accuracy.

Particle model. The particle transport model consists of equations for calculating the coordinates after a small time increment Δt of particles moving in a two-dimensional velocity field:

$$\mathbf{X}_{k+1} = \mathbf{X}_k + \mathbf{V}(\mathbf{X}_k, t_k)\Delta t , \qquad (1)$$

and

$$\tilde{\mathbf{X}}_{k+1} = \mathbf{X}_k + \mathbf{V}(\mathbf{X}_k, t_k)\Delta t\,,\ \mathbf{X}_{k+1} = \mathbf{X}_k + 0.5\left[\mathbf{V}\left(\mathbf{X}_k, t_k\right) + \mathbf{V}\left(\tilde{\mathbf{X}}_{k+1}, t_{k+1}\right)\right]\Delta t\,, \quad (2)$$

where the equations (1) and (2) correspond to the first and second approximations, respectively, $\mathbf{X}_k$ and $\mathbf{X}_{k+1}$ are the radius-vectors of a particle at times t_k and $t_{k+1} = t_k + \Delta t$, $\mathbf{V}(\mathbf{X}, t)$ is the velocity vector. To describe random motion of particles due to sub-grid turbulent diffusion, one has to add to the right hand of (1) and (2) a random displacement vector $\mathbf{X}'(\mathbf{X}, t)$.

The random displacement vector $\mathbf{X}'$ is expressed through the lateral eddy diffusivity K and time increment Δt by a random walk model:

$$\mathbf{X}' = \left(2 \cdot K \cdot \Delta t\right)^{1/2} \cdot \mathbf{A}\,, \quad (3)$$

where $\mathbf{A}$ is the Gaussian random number vector with zero mean and unit variance. For K we take $K = K\left(\mathbf{X}_k, t_k\right)$ in the first approximation and $K = 0.5\left[K\left(0.5\left(\mathbf{X}_k + \mathbf{X}_{k+1}\right), t_k\right) + K\left(0.5\left(\mathbf{X}_k + \mathbf{X}_{k+1}\right), t_{k+1}\right)\right]$ in the second approximation. Note that in the framework of this study the random walk of particles (Eq. 3) was switched off.

The necessity to apply the second approximation (2) instead of the first approximation (1) can be illustrated by a simple test case of Lagrangian floats transport in a stationary, non-divergent, eddy-like velocity field defined in polar coordinates as

$$u_\varphi = u_{\max}\left(r / r_{\text{eddy}}\right)\exp\left(1 - r / r_{\text{eddy}}\right),\ u_r = 0\,, \quad (4)$$

where r and φ are the radial and angular coordinates, and the cyclonic eddy (4) of radius r_{eddy} and maximum velocity $u_{\max}$ is placed in the coordinate system origin. Since the velocity field (4) is non-divergent, concentration of a floating tracer, being initially homogeneous, should remain homogeneous with time.

To test the Lagrangian transport models (1) and (2), we take the velocity field (4) at $u_{\max}$ = 0.3 m/s and r_{eddy} = 5 km in a round basin of radius 100×0.125 nautical mile = 23.15 km, and integrate equations (1) and (2) numerically at the time step of Δt = 10 min for the period of τ = 10 days. The velocity field is spatially resolved by 201×201 grid nodes at the lateral grid step Δx, Δy = 0.125 nautical mile and the bilinear interpolation between the nodes is applied. The test run consists of a 10-day integration of particle trajectories, provided that in the beginning 100 particles are homogeneously distributed within every grid bin (i.e., the whole round basin is homogeneously filled by particles with concentration of 100 particles per 0.125×0.125 nautical miles bin.

After the 10-day integration of the first approximation model (1), the eddy's core becomes free of the particles with the normalized concentration close to zero (see fig. 2, *a,* see an insert). The exodus of particles from the eddy's core and their gathering on the eddy's periphery is a doubtless artifact with a simple physical explanation. If the particle movement is governed by Eq. (1) at the velocity field (4), a particle that is at a distance r from the eddy's center at a time moment t will be moved tangentially by the distance of $u_\varphi \Delta t$ for the time step Δt. As a result, at time moment $t+\Delta t$, it will be found at the distance of $r + \Delta r = \sqrt{r^2 + \left(u_\phi \Delta t\right)^2} \approx r + 0.5\left(u_\phi \Delta t / r\right)^2$, being displaced away from the eddy's center by $\Delta r = 0.5\left(u_\varphi \Delta t / r\right)^2$ for the time step Δt.

If we apply the second approximation model (2), the artifact of particle exodus/gathering will be strongly suppressed (see fig. 2, *b*, see an insert): the excess/deficiency of normalized concentration at the eddy's center/periphery does not exceed 5 percent for τ = 10 days. Keeping in mind that actual changes of the normalized concentration can be as large as several orders of magnitude, the 5 percent bias is thought negligible. Note that the same values of Δt, Δx, Δy and smaller than τ = 10 days value of the advection time will be used in the next sections.

2.2 Tracers. The following parameters were used for tracers that can visualize submesoscale structures on the sea surface:

1) Temperature T, salinity S, density anomaly $\rho = \rho(T, S)$

2) Rossby number $\text{Ro} = \varsigma / f = (v_x - u_y) / f$,

where $\varsigma = v_x - u_y$ is the relative vorticity, and f is the Coriolis parameter;

3) Horizontal divergence of the flow $\text{div} = u_x + v_y$;

4) Horizontal strain (deformation rate) of the flow $\text{Strain} = \left[\left(u_x - v_y\right)^2 + \left(v_x + u_y\right)^2\right]^{1/2}$;

5) Density gradient scalar $|\nabla\rho| = (\rho_x^2 + \rho_y^2)^{1/2}$;

6) Normalized concentration of floating particles is defined as $C\left(x, y, t, \tau\right) = c\left(x, y, t, \tau\right) / c_{\text{mean}}\left(t, \tau\right)$, where $c\left(x, y, t, \tau\right)$ and $c_{\text{mean}}\left(t, \tau\right)$ is the particles concentration at a point with coordinates (x, y) and the

spatially mean value of $c(x, y, t, \tau)$ at the time moment t, provided that at the preceding time moment t—τ the particles concentration was spatially uniform ($c(x, y, t-\tau, \tau) = \text{const}$); τ is the advection time. To arrive at $C(x, y, t, \tau)$, some number of particles was uniformly deployed within every grid bin at the preceding time moment t—τ, and, using simulated Eulerian velocity components, $u(x, y, t)$ and $v(x, y, t)$, the particle trajectories for the period from t—τ to t were calculated. The concentration $c(x, y, t, \tau)$ is defined as the number of particles found within the grid bin related to the point (x, y) at the time moment t. The number of particles initially uniformly distributed within every grid bin was 2500 (i.e., $c(x, y, t-\tau, \tau)$ = 2500 particles per 0.125×0.125 nautical miles bin); the bilinear interpolation procedure was applied to calculate velocity components related to the current position of each particle. The time decrement used for integration of particle trajectories was 10 min.

7) Locations of floating particles. In addition to the normalized concentration, $C(x, y, t, \tau)$, (see above item 6), redistribution of floating particles on the sea surface can be illustrated directly, marking the current location (at the time moment t) of each particle by dot on the (x, y) plane, provided that at the preceding moment t—τ the floating particles were uniformly spaced. In this case, we generated only one particle per grid bin and placed it in the bin's center at the time moment t—τ. (Direct visual identification of a larger number of individual particles was not possible because of a finite size of markers/dots.)

8) Lagrangian Coherent Structures calculated from the Right Cauchy-Green deformation tensor and Finite-Time Lyapunov Exponent (FTLE).

In order to analyze chaotic horizontal transport in flows, the concept of Lagrangian Coherent Structures (LCS) has been introduced e.g. [30—33]. LCS provide a method to extract spatial geometrical structures that order transport in the flow. LCS divide a flow field into regions that undergo similar experience such as similar residence time within a region of interest, similar origin of fate, similar dispersion rates, etc. The LCS boundaries/manifolds are the locally strongest repelling or attracting material lines, i.e., the lines of fluid particles that cannot be crossed by ideal tracers. Therefore, they are transport barriers separating the flow into different water masses. Particles that start near the repelling manifold will separate quickly exhibiting high dispersion in forward time. Contrary, particles that start near the attracting manifold exhibit high dispersion in backward time.

Let us denote the initial position (vector) of a particle at the time moment t as $\mathbf{X} = (X_1, X_2)$ and the final position of the same particle at $t+\tau$ as $\mathbf{x} = (x_1, x_2)$. If $d\mathbf{X}$ is a line segment joining two nearby particles in the initial state and $d\mathbf{x}$ is the line segment joining the same two particles in the final state, the linear transformation between the two line segments is given by

$$d\mathbf{x} = \mathbf{F} d\mathbf{X}, \ \mathbf{F} = \frac{\partial \mathbf{x}}{\partial \mathbf{X}}, \ F_{ij} = \frac{\partial x_i}{\partial X_j},$$

where $\mathbf{F}$ or in index notation F_{ij} is the deformation gradient tensor. The Right Cauchy-Green deformation tensor is defined as

$$\mathbf{C} = \mathbf{F}^{\mathrm{T}}\mathbf{F}, \ C_{ij} = \sum_k F_{ki} F_{kj} = \sum_k \frac{\partial x_k}{\partial X_i} \frac{\partial x_k}{\partial X_j}.$$

Being a function of the initial position $\mathbf{X}$, time t and the finite-time span of advection τ, the Cauchy-Green tensor gives the square of local change in relative separation between a pair of Lagrangian particles due to finite-time advection. A physical sense of the maximum square of change in the relative separation is attributed to the largest eigenvalue of the Cauchy-Green tensor, $\lambda_{\max}\left(\mathbf{C}(\mathbf{X}, t, \tau)\right) \geq 0$, which is used to define the FTLE

$$\Lambda(\mathbf{X}, t, \tau) = \frac{1}{2\tau} \ln\left(\lambda_{\max}\left(\mathbf{C}(\mathbf{X}, t, \tau)\right)\right). \quad (5)$$

The FTLE measures a separation time scale of nearby particles. If the particles are advected forward and backward in time, the ridges of $\lambda_{\max}$ and Λ surfaces will present repelling and attracting manifolds, respectively (e.g. [33]).

In practice, the Cauchy-Green tensor was calculated in the center of every 0.125×0.125 nautical miles grid bin at the initial separation of particles of ∂X_1, ∂X_2 = 46 m for the advection time τ = 0.125, 1, and 3 days.

9) Lagrangian Coherent Structures calculated from multi-particle dispersion tensor.

Let's consider a cluster of $N = 61$ particles with coordinates $X_i(k)$, $i = 1, 2$, $k = 1, 2, \ldots, N$, initially located within a grid bin. After the advection time τ, the particles acquire coordinates $x_i(k)$. The final area occupied by the cluster can be scaled as

$$\text{Area}(\tau) = \sqrt{\mu_{\max}\mu_{\min}}\,,\ \mu_{\max} = d_{\max} / \text{M}\,,\ \mu_{\min} = d_{\min} / \text{M} \tag{6}$$

where $D_{\max} = D_{\min} = \text{M} > 0$ and $d_{\max} \geq d_{\min} > 0$, are the eigenvalues of the initial and final dispersion tensors, D_{ij} and d_{ij}, respectively:

$$D_{ij} = \overline{\left(X_i - \overline{X_i}\right)\left(X_j - \overline{X_j}\right)},\ d_{ij} = \overline{\left(x_i - \overline{x_i}\right)\left(x_j - \overline{x_j}\right)},$$

where overbar means ensemble averaging.

The LCSs can also be defined by the multi-particle dispersion tensor properties such as $\text{Area}(\tau) = \sqrt{\mu_{\max}\mu_{\min}}$, $\mu_{\max}$ and $\mu_{\min}$.

Similar to the Λ, one can introduce an analog of the FTLE based on the multi-particle dispersion tensor

$$\Lambda_{\text{disp}} = \frac{1}{2\tau}\ln\left(\mu_{\max}\right). \tag{7}$$

Both Λ and Λ_{disp} measure the relative particle separation (separation time scale).

3 Results and discussion. Simulated maps of sea surface temperature *T*, salinity *S* and density ρ for 19 August 2006 are presented in fig. 3 (see an insert). The maps of *T*, *S* and ρ characterize the relaxation phase of upwelling event along the southern shore of Gulf followed by upwelling favorable easterly wind event on 12—15 August 2006 (see [18] for details). The variability of *T*, *S* and ρ is characterized by well-defined cold/salt/dense water filaments and almost isolated spots, the latter are cyclonic vortices. Note that similar submesoscale cold filaments and cyclonic vortices were observed on satellite SST images of the Gulf of Finland in the course of upwelling events in summer 2006 (see [15] for details). Outcrops of T, S and ρ contours are concentrated on the lateral boundaries of filaments and isolated spots producing a variety of fronts. It is remarkable that narrow stripes where the density outcrops are concentrated as well as isolated cold/salt/dense water spots are always characterized by extremely high positive (cyclonic) vorticity with Ro>1 (fig. 4, top, see an insert).

In contrast to the Ro image with well-defined narrow stripes (or threads) of high cyclonic vorticity, the Div image is much more patchy (cf. fig. 4, the top and mid), though one can admit some correspondence between the Ro>1 stripes and negative values of Div, which means that the convergence of near-surface currents preferably takes place on baroclinic fronts with outcropping isopycnals. It is evident that the high cyclonic vorticity stripes coincide with the high deformation rate sites, so the Ro and Strain images look very similar (cf. fig. 4, top and bottom).

Since the high values of the lateral density gradient module $|\nabla\rho|$ correspond to the density fronts, the $|\nabla\rho|$ image actually portrays the Ro and Strain images (cf. fig. 5 and fig. 4, top and bottom).

Figs. 6 and 7 are different presentations of numerical experiments with floating particles (see the figure legends). Some comments can be formulated as follows.

1. The normalized concentration and floating particle location images provide similar portraits (with different details) of submesoscale structures for different values of the advection time of particles τ within the examined range of $0.25 \leq \tau \leq 5$ days;

2. The distributions of floating particles display a tendency to be gathered on the high Ro threads with the growth of the advection time τ;

3. The cyclonic eddies are displayed as sites where the high-concentration (and high Ro) filaments (threads) are twisted into cyclonic spirals.

4. With the decrease of τ, the normalized concentration images display a tendency to portray the Div image.

Some evidence for the latter comment (number 4) can be seen from a comparison of fig. 4 (mid) with the images of fig. 6: the smaller the τ, the higher the similarity between the normalized concentration of particles and divergence images.

The FTLE Λ for $\tau = 0.125$ and 1 day of backward and forward advection time relatively to 19 August 2006 are given in fig. 8. The Λ images for $\tau = 0.125$ and 1 day of backward time and $\tau = 0.125$ day of forward time are the most similar to the particles normalized concentration images (cf. fig. 8 and figs. 4 and 7). With the growth of forward advection time to $\tau = 1$ day, the similarity between FTLE Λ image and the surface concentration images becomes less pronounced.

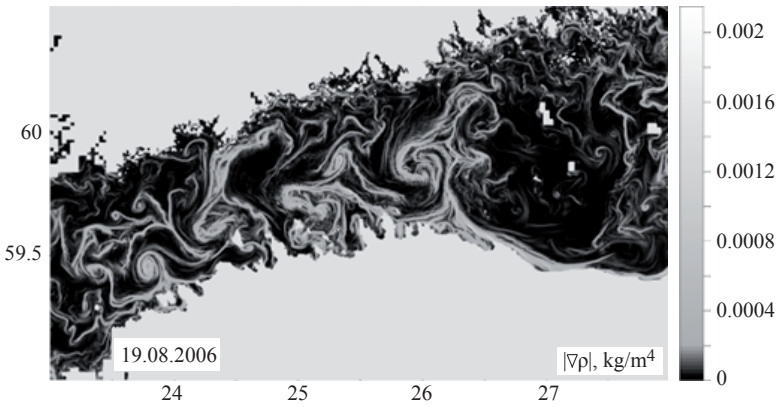

Fig. 5. The same as in figs. 3 and 4 but for the horizontal density gradient module $|\nabla\rho|$.

Рис. 5. То же, что на рис. 3 и 4, но для модуля горизонтального градиента плотности $|\nabla\rho|$.

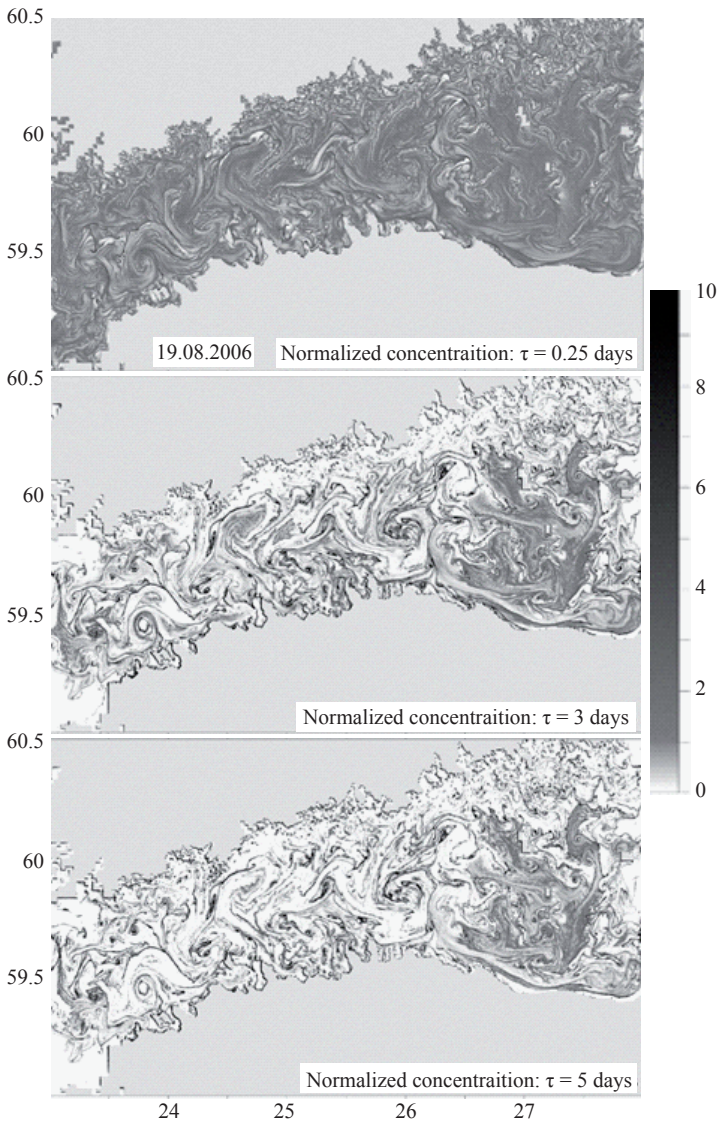

Fig. 6. The same as in Figs. 3—5 but for normalized concentration of a floating particles, uniformly distributed on the sea surface 6 hours (top), 3 days (mid), and 5 days (bottom) before 19 August 2006.

Рис. 6. То же, что на рис. 3—5, но для нормализованной концентрации плавающих частиц, равномерно распределенных на поверхности моря за 6 часов (сверху), 3 сут (в середине) и 5 сут (внизу) до 19 августа 2006 г.

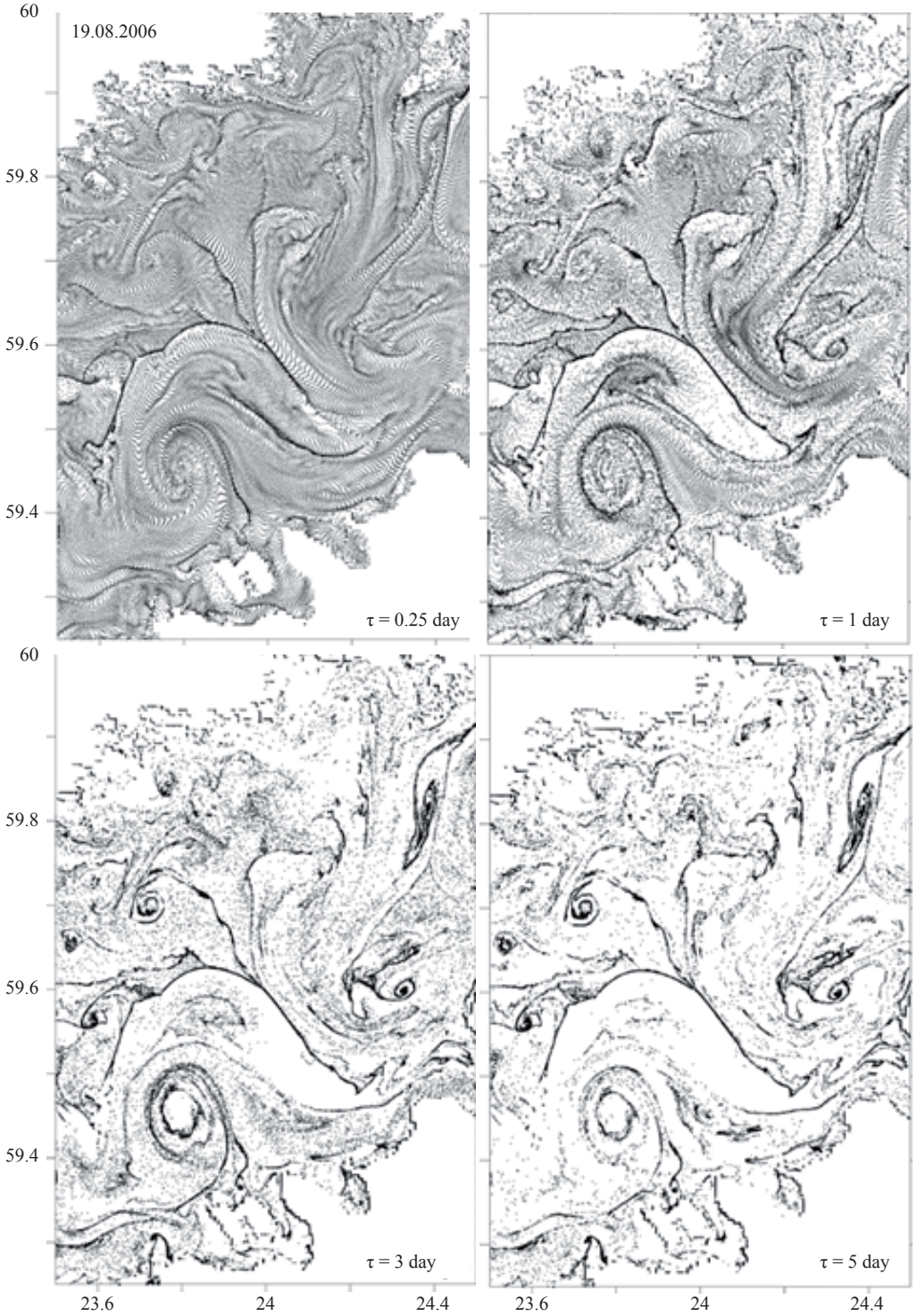

Fig. 7. Simulated sea surface images created by floating particles uniformly deployed 6 hours, 1 day, 3 and 5 days before 19 August 2006. The location of each particle is depicted by dot. Only a zoomed fragment of the Gulf (see fig. 1) is shown to make it possible seeing of individual particles.

Рис. 7. Модельные изображения морской поверхности, созданные плавающими частицами, равномерно распределенными за 6 часов, 1, 3 и 5 сут до 19 августа 2006 г. Положение каждой частицы изображено точкой. Показан только увеличенный фрагмент Финского залива (см. рис. 1), что позволяет видеть отдельные частицы.

The Λ_{disp} images are similar to the Λ images both for small and large values of τ (cf. fig. 9 and fig. 8). For small τ, the high-concentration threads are characterized by high Λ and Λ_{disp}.

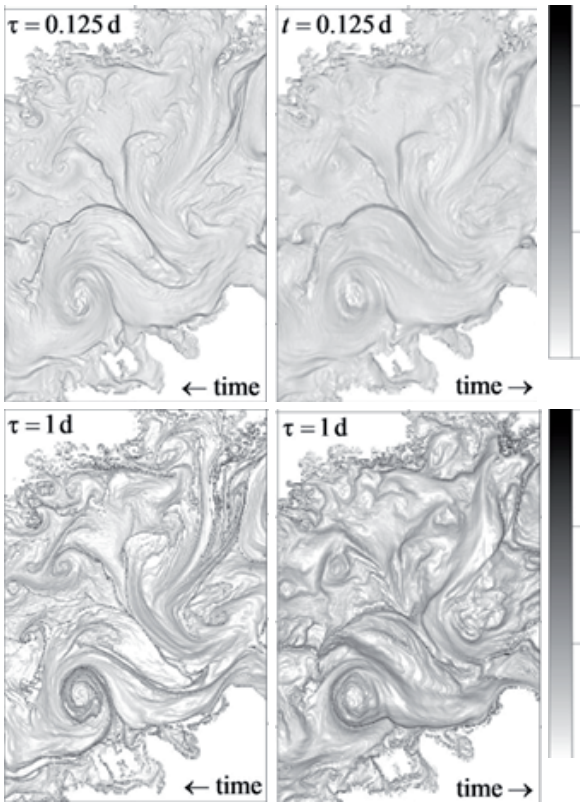

Fig. 8. The FTLE Λ for τ = 0.125 and 1 day (top and bottom, respectively) of backward (left) and forward (right) advection time relative to 19 August 2006.

Рис. 8. Карта конечно-временного показателя Ляпунова Λ (FTLE) при τ = 0.125 и 1 сут (сверху и снизу соответственно) и интегрировании назад (слева) и вперед (справа) по времени относительно 19 августа 2006 г.

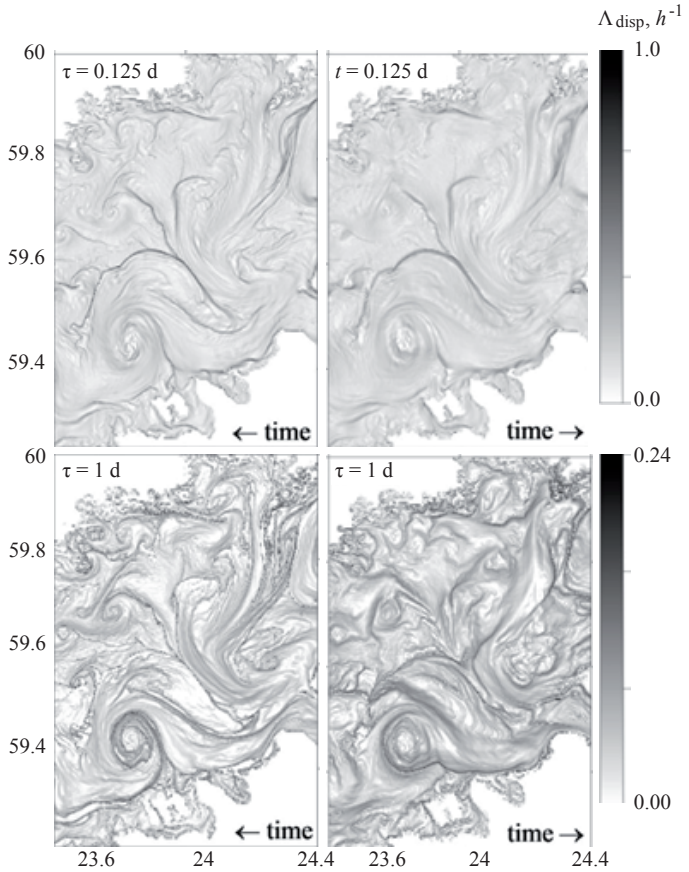

Fig. 9. The same as in Fig. 8 but for Λ_{disp}.

Рис. 9. То же, что на рис. 8, но для Λ_{disp}.

Statistics of normalized concentration fluctuations. Here we will consider statistical characteristics of submesoscale fluctuations of normalized concentration, $C(x,y,t,\tau) = c(x,y,t,\tau) / c_{\text{mean}}(t,\tau)$, such as probability density functions and statistical moments, depending on the advection time τ.

Probability density function. [34] suggested the log-normal statistical distribution for a tracer concentration in a turbulent flow by the following argumentation. He considered a cloud of marked fluid released in an initial concentration C_0 into a turbulent field. Concentration of a passive tracer in a small parcel of the cloud can be considered as a result of a number of diluting impulses, in each of which the parcel is mixed with a certain proportion of ambient fluid. Each such impulse produces a drop in concentration by a random factor $0 < \xi_i < 1$, leading to a decreasing succession of concentration values such as

$$C = C_0,\ \xi_1 C_0,\ \xi_2 \xi_1 C_0,\ \xi_3 \xi_2 \xi_1 C_0, \ldots,$$

so that

$$\ln(C / C_0) = \ln \xi_1 + ln\ \xi_2 + \ldots + ln\ \xi_n .$$

Since $\ln(C / C_0)$ is a sum of a number of independent random variables of the same order of magnitude, it should by the Central Limit Theorem tend to a normal distribution for a large number of diluting impulses *n*.

In our case the initial concentration of floating particles is uniform, and the fluctuations cannot appear due to diluting impulses. Instead, they appear due to multiple local events of horizontal convergence/divergence of flow velocity whose effect can be thought of as the multiplicative of many independent random variables each of which is positive, implying the log-normality.

Probability Density Functions for the normalized concentration of floating particles in the Gulf and for its natural logarithm, $\mathrm{PDF}\left(C / C_{\mathrm{mean}}\right)$ and $\mathrm{PDF}\left(\ln\left(C / C_{\mathrm{mean}}\right)\right)$, calculated at different values of τ for 19 August 2006, is shown in figs. 10 and 11, respectively. To eliminate the effect of boundaries, we took into account the concentration estimates only for bins where the sea depth is larger than 25 m. In addition, the mean μ, variance $\sigma^2 = M_2$, skewness $\mathrm{Skew} = M_3 / \sigma^3$ and excess kurtosis $\mathrm{Excess} = M_4 / \sigma^4 - 3$ of statistical distributions $\mathrm{PDF}\left(C / C_{\mathrm{mean}}\right)$ and $\mathrm{PDF}\left(\ln\left(C / C_{\mathrm{mean}}\right)\right)$, where

$$\mu = \int_{-\infty}^{\infty} x\mathrm{PDF}(x)dx,\ M_n = \int_{-\infty}^{\infty} (x-\mu)^n\ \mathrm{PDF}(x)dx,\ n = 2,3,4,$$

are statistical moments, are presented in Table. (Note that, by definition, μ = 1 for the normalized concentration C / C_{mean}, so it has been dropped from the table).

For comparison, we also showed the log-normal PDF curves

$$\mathrm{PDF}(x) = \mathrm{PDF}(\ln x)\frac{d\ln(x)}{dx} = \frac{1}{x\sigma\sqrt{2\pi}}\exp\left[-\frac{(\ln x-\mu)^2}{2\sigma^2}\right] \quad (8)$$

at different values of standard deviation σ and zero mean value μ = 0 of ln*x*. Note that the log-normal distribution (8) obeys an asymptotic relationship

$$\mathrm{PDF}(x) \approx \frac{e^{-\mu}}{\sigma\sqrt{2\pi}}\exp\left[-\frac{\left(e^{-\mu}x-1\right)^2}{2\sigma^2}\right] \text{ at } \sigma << 1 \text{ and } \mathrm{PDF}(x) = \frac{1}{x\sigma\sqrt{2\pi}} \text{ at } \sigma >> 1. \quad (9)$$

The probability distribution of C / C_{mean} is characterized by large positive, fast time-growing values of Skew and Excess: Skew = 1.53, Excess = 15.1 for τ = 0.5 h and Skew = 314.7, Excess = $1.3\cdot10^5$ for τ = 10 days. The probability distribution of $\ln\left(C / C_{\mathrm{mean}}\right)$ is characterized by mostly negative, relatively close to zero values of skewness |Skew| < 1 while the kurtosis excess being positive approaches to zero with the growth

Statistics of probability distributions of C / C_{mean} and $\ln\left(C / C_{\mathrm{mean}}\right)$ for different values of the advection time τ. The α_0 is the share of zero concentration bins

Статистические моменты функции плотности вероятности нормализованной концентрации C / C_{mean} и логарифма нормализованной концентрации $\ln\left(C / C_{\mathrm{mean}}\right)$ для различных значений времени адвекции τ. Величина α_0 дает долю площади поверхности моря с нулевой концентрацией частиц

τ, day	α_0	σ^2	Skew	Excess	μ_ln	σ^2_ln	Skew_ln	Excess_ln
0.0208	0	0.00463	1.53	15.1	0.00223	0.00441	0.343	11.1
0.0417	0	0.0174	2.18	22.1	0.008	0.0157	0.165	9.15
0.0832	3.16E-6	0.0631	3.12	34.5	-0.0268	0.0524	-1.17	6.92
0.125	2.21E-5	0.129	3.76	44.4	-0.0514	0.101	-0.309	8.35
0.167	3.16E-5	0.208	4.28	51.6	-0.0781	0.155	-0.361	5.6
0.25	6.32E-5	0.38	5.59	84.2	-0.129	0.261	-0.578	5.25
0.333	1.67E-4	0.576	8.05	208.9	-0.172	0.352	-0.662	4.89
0.417	2.12E-4	0.805	11.5	515	-0.212	0.44	-0.773	5.22
0.5	2.97E-4	1.03	14.3	815.6	-0.25	0.524	-0.859	5.44
0.625	6.35E-4	1.39	15.8	897.9	-0.309	0.662	-0.931	5.07
0.75	0.00103	1.79	15.4	697	-0.366	0.794	-0.945	4.74
1	0.00131	2.74	17.9	731.6	-0.468	1.03	-0.928	3.89
2	0.00932	10.7	56.1	9393.5	-1.04	2.58	-0.91	2.02
3	0.0266	22.2	81.5	16228.4	-1.42	3.49	-0.66	0.859
5	0.0873	46.1	65.6	7604.5	-2.19	5.66	-0.361	0.371
10	0.224	201.1	314.7	127249.7	-2.57	6.37	-0.143	-0.664

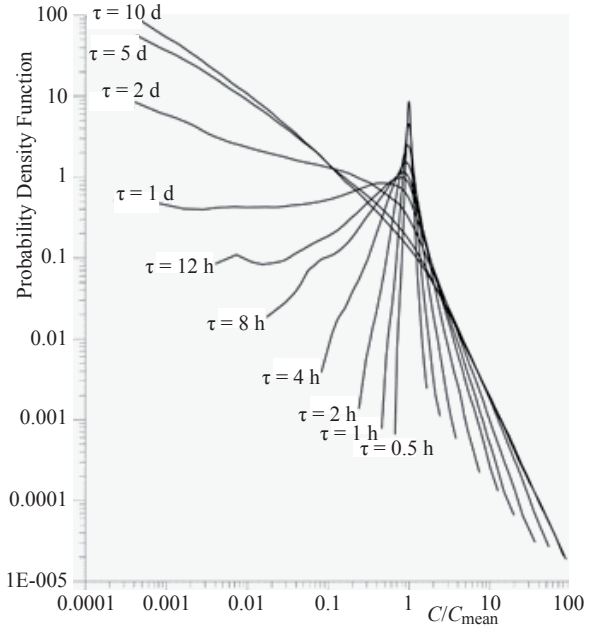

Fig. 10. Probability Density Function of the normalized concentration of floating particles, $\mathrm{PDF}\left(C / C_{\mathrm{mean}}\right)$, calculated at different values of τ for 19 August 2006.

Рис. 10. Функция плотности вероятности нормализованной концентрации плавающих частиц $\mathrm{PDF}\left(C / C_{\mathrm{mean}}\right)$, рассчитанная при разных значениях τ для 19 августа 2006 г.

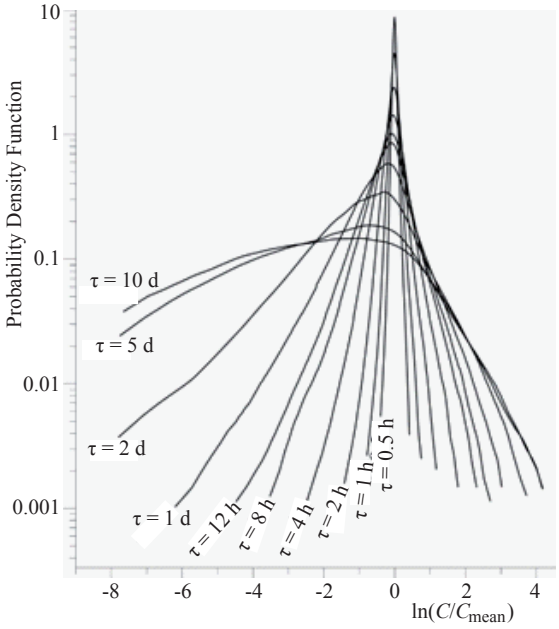

Fig. 11. The same as in fig. 10 but for natural logarithm of the normalized concentration of floating particles.

Рис. 11. То же, что на рис. 10, но для натурального логарифма нормализованной концентрации частиц.

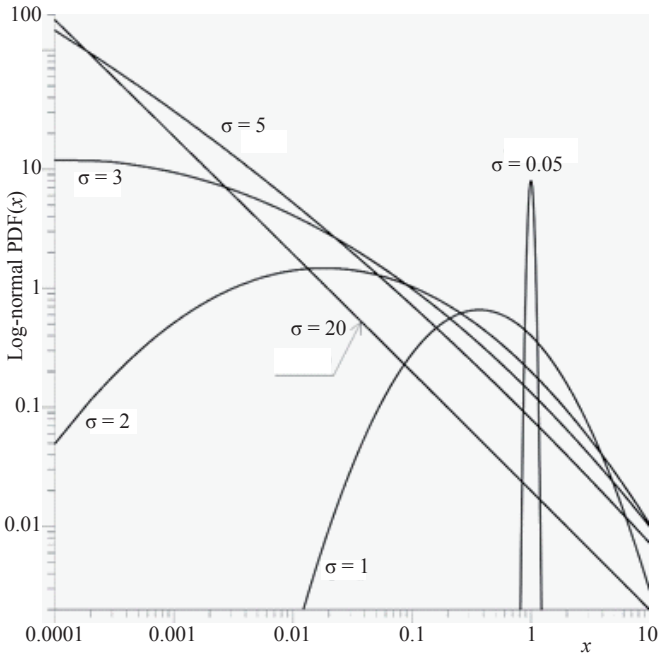

Fig. 12. Log-normal Probability Density Function PDF(x) depending on standard deviation σ.

Рис. 12. Логнормальная функция плотности вероятности PDF(x) при различной величине стандартного отклонения σ.

of advection time τ. Therefore, we can cautiously assert approximate log-normality of the normalized concentration C / C_{mean} at large τ (remember that for the normal probability distribution Skew = 0, Excess = 0).

Evolution of the shape of probability density function of C / C_{mean} is characterized by the transformation of a domelike curve at small τ (and therefore small σ) to a monotonically descending curve at large τ (and therefore large σ) in a vicinity of $C / C_{\text{mean}} = 1$. Qualitatively similar evolution is displayed by the log-normal distribution (8) for σ << 1 and σ >> 1, respectively.

Standard deviation of the normalized concentration versus advection time. The rate at which the initially homogeneous distribution of floating particles forms clusters due to submesoscale advection can be characterized by an advection time dependence of the standard deviation of normalized concentration, $\sigma(\tau) \equiv \sqrt{\sigma^2(\tau)}$ (see fig. 13 *a* were curves of simulated σ(τ) dependencies are presented in the log-log space for an advection time range 0.5 h ≤ τ ≤ 12.4 days at different initial/final time moments and model grid sizes of 0.125 and 0.5 nautical miles). All the curves, being at different levels of the σ coordinate, display nearly identical linear growth in the log-log space (actually nearly power growth with the value of power index about 0.9). Note that a quadruple decrease in the grid size from 0.5 to 0.125 nautical miles (i.e., the quadruple increase of model resolution) results in an approximately twofold increase of σ (cf. curves with identical but filled and blanked symbols in fig. 13 *a*).

Keeping in mind that in a 2D non-divergent velocity field the normalized concentration of a tracer being uniformly distributed initially, remains uniform regardless of the advection time τ, the σ(τ) curves are expected to be scaled (i.e., reduced to a single curve) by some characteristic of the intensity of divergence fluctuations. For the intensity of divergence fluctuations, one can choose the standard deviation of the 2D velocity divergence, σ_{div} calculated by spatial averaging of Div fluctuations over the same domain that was used to calculate σ(τ) and by temporal averaging over the advection period τ. Doing like that, we arrived at non-dimensional curves of σ versus non-dimensional advection time $\sigma_{\text{div}}\tau$ (see fig. 13 *b*). An expected but still exciting result is the reduction of the σ(τ) curves to a single straight line at small values of $\sigma_{\text{div}}\tau$ with a simple asymptotic relationship $\sigma = \sigma_{\text{div}}\tau$, $\sigma_{\text{div}}\tau << 1$.

Note that the asymptotic relationship (9) can be derived from a balance equation for floating particles concentration

$$\frac{\partial C}{\partial t} + \frac{\partial (C u_i)}{\partial x_i} = 0, \quad i = 1, 2 . \tag{10}$$

Resolve velocities and particles concentration into mean and fluctuating components:

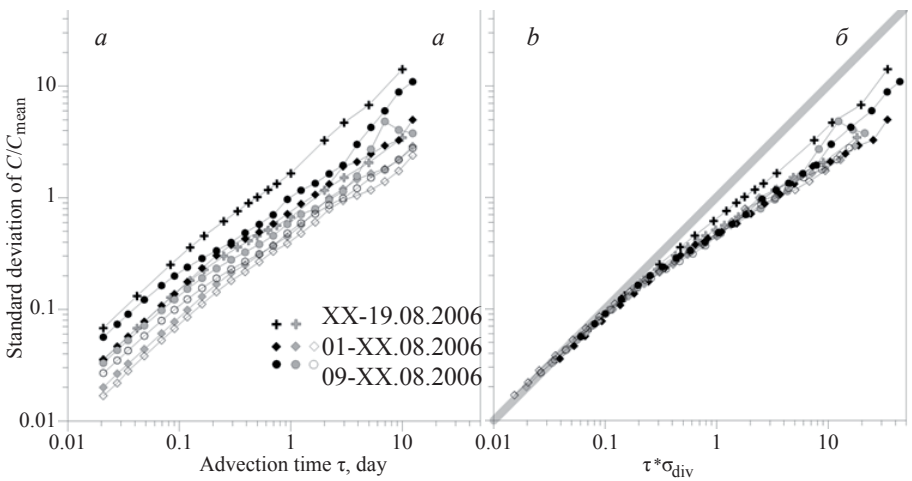

Fig. 13. Standard deviation of the normalized concentration vs. advection time τ (*a*); the same as (*a*) but vs. τ multiplied by the standard deviation of flow divergence (*b*). Black-, grey-, and white-filled symbols refer to the 0.125, 0.5, and 1 nautical mile grid runs, respectively.

Рис. 13. Зависимость стандартного отклонения нормализованной концентрации от времени адвекции τ (*а*); то же самое, что (*а*), но в зависимости от произведения времени адвекции τ на стандартное отклонение дивергенции скорости (*б*). Символы с черным, серым и белым наполнением соответствуют численным расчетам по модели с шагом сетки 0.125, 0.5, и 1.0 морской мили соответственно.

$$u_i = \overline{u}_i + u_i',$$
$$C = \overline{C} + C'$$

Suggesting that $\overline{u}_i = 0,\ \overline{C} = \text{const} > 0$, taking ensemble means of both sides of equation (10), and subtracting the average from the original equation, we get an equation for concentration fluctuation

$$\frac{\partial C'}{\partial t} = -\overline{C}\frac{\partial u_i'}{\partial x_i} - C'\frac{\partial u_i'}{\partial x_i} - u_i'\frac{\partial C'}{\partial x_i} \tag{11}$$

Keeping in mind that we start from a homogeneous distribution of floating stuff ($C' = 0$, $\overline{C} = \text{const} > 0$ at $t = 0$), at t→+0 the second and third terms in the right hand of (11) can be dropped since $C'/\overline{C} < 1$. One can integrate (11) to get

$$\frac{C'}{\overline{C}} = -\frac{\partial u_i'}{\partial x_i}t \text{ at } C'/\overline{C} < 1,$$

which is identical to the asymptotic relationship $\sigma = \sigma_{\text{div}}\tau,\ \sigma_{\text{div}}\tau << 1$.

A criterion for finite-time clustering. The balance equation for floating particles concentration (10) can be re-written as

$$\frac{dC}{dt} = -C\,\text{div}\left(\mathbf{u}\right) = -C\frac{\partial u_i}{\partial x_i},\ i = 1,\ 2, \text{ or } \frac{d\ln C}{dt} = -\text{div}\left(\mathbf{u}\right), \tag{10'}$$

where $\frac{dC}{dt} = \frac{\partial C}{\partial t} + u_i\frac{\partial C}{\partial x_i}$ is the material time derivative of concentration. Equation (10') can be integrated versus time along a particle trajectory to get

$$C(\mathbf{x},t) = C\left(t-\tau \mid \mathbf{x},t\right)\exp\left[\int_t^{t-\tau}\text{div}\left(\mathbf{u}\left(t' \mid \mathbf{x},t\right)\right)dt'\right], \tag{12}$$

where $A\left(t' \mid \mathbf{x},t\right)$ denotes the value of a property A at time moment t' for a Lagrangian particle that had radius-vector $\mathbf{X}$ at time moment t. The quadrature solution (12) says that concentration of floating stuff at a material point ($\mathbf{x}$, t) equals the concentration at the same material point in the preceding time moment $t-\tau$ multiplied by the exponent of the backward time integral of the Lagrangian velocity divergence for the time interval [t, $t-\tau$]. Since in accordance to (12) $C\left(\mathbf{x},t\right) > C\left(t-\tau \mid \mathbf{x},t\right)$ corresponds to $\int_t^{t-\tau}\text{div}\left(\mathbf{u}\left(t' \mid \mathbf{x},t\right)\right)dt' > 0$ the criterion of finite-time clustering (FTC) for an advection time period τ preceding the time moment t is

$$\text{FTC}\left(\mathbf{x},t,\tau\right) = \int_t^{t-\tau}\text{div}\left(\mathbf{u}\left(t' \mid \mathbf{x},t\right)\right)dt' > 0. \tag{13}$$

The validity of (12) and, therefore, (13) is confirmed in fig. 14 where the normalized concentration of particles in the Gulf of Finland for time moment of 19 August 2006 and advection time τ = 1 day calculated by forward-time integration of trajectories of uniformly distributed particles with an initial concentration of 2500 particles per 232×232 m bin is shown versus exp(FTC($\mathbf{x}$, t, τ)) calculated using backward-time integration of Lagrangian velocity divergence for a particle placed in the center of every bin (i.e., only one particle per bin). The maps of the normalized concentration and exp(FTC($\mathbf{x}$, t, τ)) in fig. 14 are practically identical which validates the FTC criterion (13).

4 Conclusions

To study the effect of submesoscale dynamics on clustering of floating stuff on the sea surface, the trajectories of synthetic surface floats were calculated. The velocity fields were simulated for a period of strong upwelling events in the Gulf of Finland in summer 2006 using a circulation model with a very high horizontal resolution of 0.125 nautical miles [18]. The trajectories were calculated using an advanced advection scheme; it was tested that if the scheme was applied to spatially uniformly distributed particles in a 2D non-divergent velocity field, then the uniformity of the particle concentration was conserved. The synthetic floats were initially uniformly distributed on the sea surface with concentration up to 2500 particles per grid bin (or 1 particle per 4.6×4.6 m which corresponds to approximately 2 billion particles in total within the Gulf). Such numerical experiments with a huge amount of synthetic floating particles made possible to follow the evolution of particle

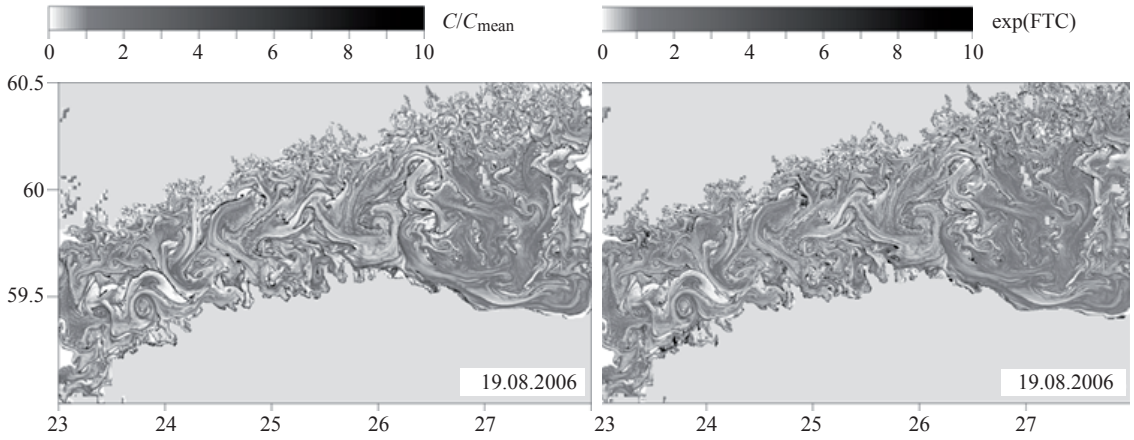

Fig. 14. Normalized concentration (left) and exp(FTC) (right) calculated for time moment 19 August 2006 and advection time $\tau = 1$ day.

Рис. 14. Карты нормализованной концентрации (слева) и параметра exp(FTC) (справа), рассчитанные для момента времени 19 августа 2006 г. при времени адвекции $\tau = 1$ сут.

concentration field, its probability density function and statistical moments depending on the advection time, and thereby thoroughly characterize the process of clustering.

For a relatively short time of advection τ (of the order of one day), the synthetic particles were found to gather within narrow, elongated stripes. The cluster locations were characterized by extremely high, positive values of vorticity, Finite-Time Lyapunov Exponent, and lateral thermohaline gradients module (i.e., thermohaline fronts). The clustering rate, defined as the time derivative of the standard deviation of normalized particle concentration, tended asymptotically at small τ to the standard deviation of flow divergence. The standard deviation of flow divergence, in its turn, displayed a considerable growth with the refinement of the model grid, confirming the paramount role of submesoscale dynamics in clustering of floating stuff. At large τ, the probability density function of floating particle concentration was shown to tend to lognormality. Based on the backward-time integration of the Lagrangian velocity convergence, a criterion for finite-time clustering was introduced.

In conclusion, the effect of submesoscale dynamics on clustering of floating stuff on the sea surface can be reduced to two specific features. First, the clustering sites are characterized by extremely high cyclonic vorticity, and secondly, submesoscale motions result in a considerable increase in clustering rate due to the increase in fluctuations of the horizontal velocity divergence.

This work was supported by institutional research funding IUT 19-6 of the Estonian Ministry of Education and Research. Victor Zhurbas was supported by the state assignment of FASO Russia (theme No 0149-2018-0002). The parallel implementation of the original POM was done by Dr. Antoni Jordi and is documented in Jordi & Wang (2012). An allocation of computing time from the High Performance Computing cluster at the Tallinn University of Technology is gratefully acknowledged.

References

1. *Thomas L. N., Tandon A., Mahadevan A.* Submesoscale Processes and Dynamics. In Hecht, M.W., Hasumi, H. (Eds.) Ocean Modeling in an Eddying Regime. *Geophysical Monograph Series.* 2008, 177, Washington, American Geophysical Union, 10.1029/177GM04, 17—38.
2. *Dencausse G., Morrow R., Rogé M., Fleury S.* Lateral stirring of large-scale tracer fields by altimetry. *Ocean Dynamics.* 2014, 64, 61—78. doi:10.1007/s10236-013-0671-8.
3. *Gaube P., McGillicuddy D. J.* The influence of Gulf Stream eddies and meanders on near-surface chlorophyll. *Deep-Sea Research Part I: Oceanographic Research Papers,* 2017, 122, 1—16.
4. *Karimova S.* Spiral eddies in the Baltic, Black and Caspian seas as seen by satellite radar data. *Advances in Space Research.* 2012, 50, 1107—1124.
5. *Haza A. C., Özgökmen T. M., Hogan P.* Impact of submesoscales on surface material distribution in a gulf of Mexico mesoscale eddy. *Ocean Modelling.* 2016, 107 (2016), 28—47.
6. *Bergström S., Alexandersson H., Carlsson B., Fosefsson W., Karlsson K. G., Westring G.* Climate and hydrology of the Baltic Sea. In: Wulff F., Rahm L. & Larsson P. (eds.), *A System Analysis of the Baltic Sea.* Ecological Studies 148, Springer-Verlag, Berlin Heidelberg New York, 2001, 75—112.

7. *Alenius P., Myrberg K., Nekrasov A.* The physical oceanography of the Gulf of Finland: a review. *Boreal Env. Res.* 1998, 3, 97—125.
8. *Kahru M., Håkansson B., Rud O.* Distributions of the sea-surface temperature fronts in the Baltic Sea as derived from satellite imagery. *Cont. Shelf Res.* 1995, 15, 663—679.
9. *Lehmann A., Myrberg K., Höflich K.* A statistical approach to coastal upwelling in the Baltic Sea based on the analysis of satellite data for 1990—2009. *Oceanologia.* 2012, 54(3), 369—393. doi:10.5697/oc.54-3.369
10. *Uiboupin R., Laanemets J.* Upwelling Parameters From Bias-Corrected Composite Satellite SST Maps in the Gulf of Finland (Baltic Sea). *IEEE Geoscience and Remote Sensing Letters.* 2015, 12 (3), 592—596. doi: 10.1109/LGRS.2014.2352397
11. *Vahtera E., Laanemets J., Pavelson J., Huttonen M., Kononen K.* Effect of upwelling on the pelagic environment and bloom-forming cyanobacteria in the western Gulf of Finland, Baltic Sea. *J. Mar. Syst.* 2005, 58, 67—82.
12. *Lips U., Lips I.* Bimodal distribution patterns of motile phytoplankton in relation to physical processes and stratification (Gulf of Finland, Baltic Sea). *Deep-Sea Research, Part II: Topical Studies in Oceanography,* 2014, 101, 107—119.
13. *Myrberg K., Andrejev O.* Main upwelling regions in the Baltic Sea — a statistical analysis based on three-dimentional modelling. *Boreal Environ. Res.* 2003, 8, 97—112.
14. *Zhurbas V. M., Laanemets J., Vahtera E.* Modeling of the mesoscale structure of coupled upwelling/downwelling events and the related input of nutrients to the upper mixed layer in the Gulf of Finland, Baltic Sea. *J. Geophys. Res.* 2008, 113, C05004. doi: 10.1029/2007JC004280
15. *Laanemets J., Väli G., Zhurbas V., Elken J., Lips I., Lips U.* Simulation of mesoscale structures and nutrient transport during summer upwelling events in the Gulf of Finland in 2006. *Boreal Environ. Res.* 2011, 16(A), 15—26.
16. *Capet X., McWilliams J. C., Molemaker M. J., Shchepetkin A.* Mesoscale to Submesoscale Transition in the California Current System. Part I: Flow Structure, Eddy Flux, and Observational Tests. *J. Phys. Oceanogr.* 2008, 38, 29—43.
17. *Gula J., Molemaker M. J., McWilliams J. C.* Submesoscale Cold Filaments in the Gulf Stream. *J. Phys. Oceanogr.* 2014, 44, 2617-2643. doi:10.1175/JPO-D-14-0029.1
18. *Väli G., Zhurbas V., Lips U., Laanemets J.* Submesoscale structures related to upwelling events in the Gulf of Finland, Baltic Sea (numerical experiments). *J. Mar. Syst.* 2017, 171, 31—42. doi:10.1016/j.jmarsys.2016.06.010
19. *Kalda J., Soomere T., Giudici A.* On the compressibility of the surface currents in the Gulf of Finland, the Baltic Sea. *J. Mar. Sys.* 2014, 129, 56—65.
20. *Blumberg A. F., Mellor G. L.* Diagnostic and prognostic numerical calculation studies of the South Atlantic Bight. *J. Geophys. Res.* 1983, 88, 4579—4592.
21. *Oey L., Chang Y-L., Lin Y-C., Chang M-C., Xu F., Lu H-F.* ATOP — The Advanced Taiwan Ocean Prediction System Based on the mpiPOM. Part 1: Model Descriptions, Analyses and Results. *Terr. Atmos. Ocean. Sci.* 2013, 24, 137—158.
22. *Mellor G.L., Yamada T.* Development of a turbulence closure model for geophysical fluid problems. *Rev. Geophys. Space Phys.* 1982, 20 (4), 851—875.
23. *Smagorinsky J.* General circulation experiment with the primitive equations. I. The basic experiment. *Mon. Weather Rev.* 1963, 91, 99—164.
24. *Seifert T., Tauber F., Kayser B.* A high resolution spherical grid topography of the Baltic Sea – 2nd edition, Baltic Sea Science Congress, Stockholm 25—29 November 2001, Poster #147, www.io-warnemuende.de/iowtopo, 2001.
25. *Andrejev O., Soomere T., Sokolov A., Myrberg K.* The role of spatial resolution of a three-dimensional hydrodynamic model for marine transport risk assessment. *Oceanologia.* 2011, 53 (1-TI), 309—334.
26. *Andrejev O., Sokolov A., Soomere T., Värv R., Viikmäe B.* The use of high-resolution bathymetry for circulation modelling in the Gulf of Finland. *Est. J. Eng.* 2010, 16 (3), 187—–210.
27. *Männik A., Merilain M.* Verification of different precipitation forecasts during extended winter-season in Estonia. *HIRLAM Newsletter.* 2007, 52, 65—70.
28. *Funkquist L.* HIROMB, an operational eddy-resolving model for the Baltic Sea. *Bulletin of the Maritime Institute in Gdansk XXVIII.* 2001, 7—16.
29. *Marshall J., Hill C., Perelman L., Adcroft A.* Hydrostatic, quasi-hydrostatic, and nonhydrostatic ocean modeling. *J. Geophys. Res.* 1997, 102(C3), 5733—5752.
30. *Haller G.* Finding finite-time invariant manifolds in two-dimensional velocity fields. *Chaos.* 2000, 10(1), 99—108.
31. *Ide K., Kuznetsov L.* Jones C.K.R.T. Lagrangian data assimilation for point vortex systems. 2002. *J. Turbul.* 3, 053.
32. *Lapeyre G.* Characterization of finite-time Lyapunov exponents and vectors in two-dimensional turbulence. *Chaos.* 2002, 12(3), 688—698.
33. *Huhn F., von Kameke A., Allen-Perkins S., Montero P., Venancio A., Pérez-Muñuzuri V.* Horizontal Lagrangian transport in a tidal-driven estuary - transport barriers attached to 34 prominent coastal boundaries. *Con. Shelf Res.* 2012, 39—40, 1—13.
35. *Csanady G. T.* Turbulent Diffusion in the Environment. *D. Reidel, Norwell, Mass.,* 1974, 48 p.

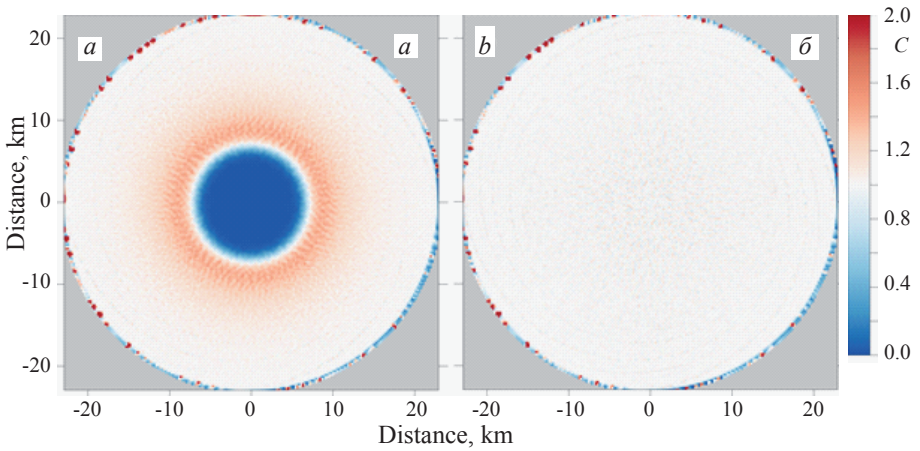

Fig. 2. Normalized concentration of particles for a test case with a stationary, non-divergent eddy-like velocity field at τ = 10 days: *a* – the first approximation model (Eq. 1), *b* – the second approximation model (Eq. 2).

Рис. 2. Нормализованная концентрация частиц в случае теста со стационарным бездивергентным вихреподобным полем скорости при τ = 10 сут: *а* — модель первого приближения (уравнение 1), *б* — модель второго приближения (уравнение 2).

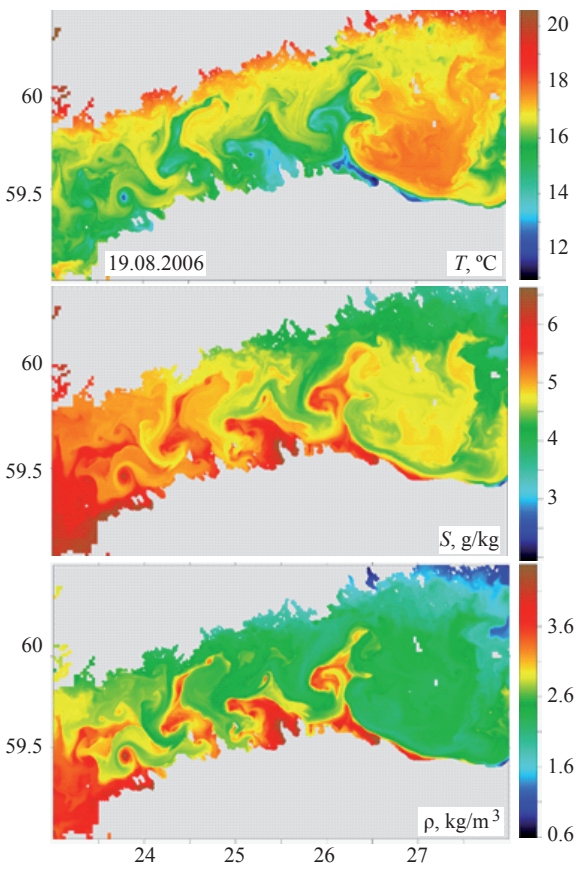

Fig. 3. Simulated maps of temperature *T*, salinity *S*, and density anomaly ρ in the surface layer of the Gulf of Finland on 19 August 2006.

Рис. 3. Модельные карты температуры *T*, солености *S* и аномалии плотности ρ в поверхностном слое Финского залива на 19 августа 2006 г.

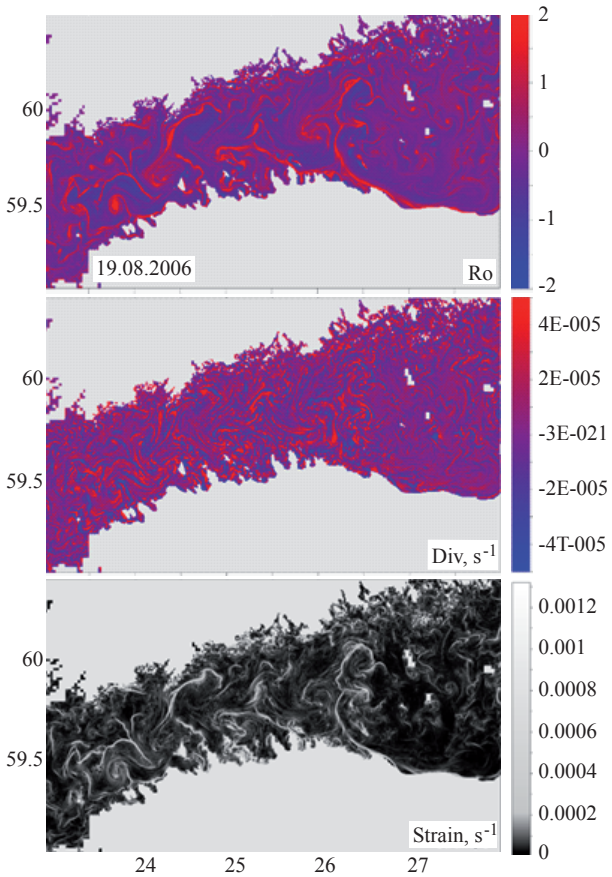

Fig. 4. The same as in Fig. 3 but for the Rossby number Ro, divergence of velocity of current, Div, and deformation rate Strain.

Рис. 4. То же, что на рис. 3, но для числа Россби Ro, дивергенции скорости течения, Div и скорости деформации Strain.